Available online at www.sciencedirect.com
SCIENCE DIRECT®
ELSEVIER
Solid-State Electronics 49 (2005) 769–773
SOLID-STATE ELECTRONICS
www.elsevier.com/locate/sse

Ion implantation dose high-resolution monitoring in Si wafers using laser infrared photothermal radiometry with lock-in common-mode-rejection demodulation

Andreas Mandelis *, Felipe Rabago [1]

Center for Advanced Diffusion-Wave Technologies, Department of Mechanical and Industrial Engineering, University of Toronto, 5 King's College Road, Toronto, Ont., Canada M5S 3G8

Received 16 November 2001; received in revised form 19 October 2004

The review of this paper was arranged by Prof. C. Hunt

Abstract

Frequency-scanned and lock-in common-mode-rejection demodulation schemes were used with laser infrared photothermal radiometric (PTR) detection of B^+, P^+, and As^+ ion-implanted Si wafers, with or without surface-grown oxides. The implantation energy was 100 keV with doses in the range 1×10^{11}–1×10^{13} ions/cm^2. The lock-in common-mode-rejection demodulation (CMRD) scheme exhibited superior signal resolution in all cases where the conventional frequency-scan signals were essentially overlapped. These were B^+-implants in the dose range 1×10^{12}–1×10^{13} ions/cm^2, and P^+-implants in the 10^{12} ions/cm^2 range.
© 2005 Elsevier Ltd. All rights reserved.

Very recently a novel harmonic common-mode-rejection (CMR) lock-in amplifier (LIA) pulse waveform demodulation scheme was introduced [1,2]. This particular repetitive waveform is shown in Fig. 1. It takes advantage of the details of the demodulation mechanism in conventional lock-in amplifiers [3], resulting in complete suppression of baseline signals. The demodulated LIA signal output expected from an input double square waveform of equal durations $\tau_1 = \tau_2$, is ideally zero. This occurs because the demodulated LIA output signal with a long filter time-constant compared to the waveform repetition period, is the time-integral (area) of the input waveform during the first half cycle minus the integral (area) of the input waveform during the second half cycle [3]. For identical half-waveforms and zero instrumental phase delay (alignment of the LIA reference square-wave rising edge with the onset of the external incident waveform), this signal generation scheme implies that equal areas are swept along the time axis. Therefore, the result of the signal demodulation (integral/area subtraction between [0, T/2] and [T/2, T] segments) is zero for all types of waveforms. This signal generation principle can be thought of as the temporal analog of destructive interference due to spatial superposition of two out-of-phase waves. The main advantage of CMR demodulation (CMRD) is the suppression of LIA signal baselines, which, in turn, enhances the dynamic range of the instrument. An application of CMRD to photothermal radiometric detection [2] has shown considerable measurement resolution improvement in cases where minute changes in sample thermophysical properties produce only very small signal differences. These differences are usually imperceptible under conventional square- or

* Corresponding authors. Tel.: +1 416 978 5106; fax: +1 416 266 7867.
E-mail address: mandelis@mie.utoronto.ca (A. Mandelis).
[1] On leave from: Universidad Autonoma di San Luis Potosi, S.L.P., Mexico.

0038-1101/$ - see front matter © 2005 Elsevier Ltd. All rights reserved.
doi:10.1016/j.sse.2005.01.013

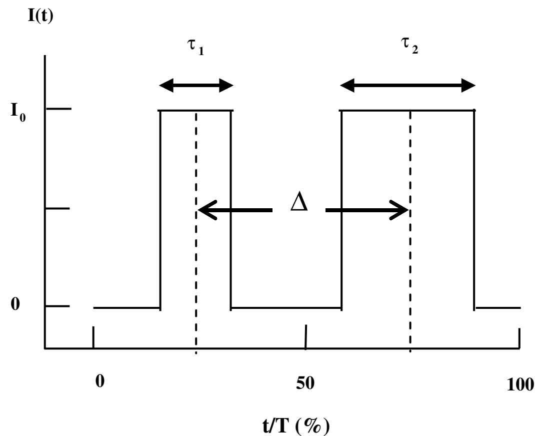

Fig. 1. CMRD optical excitation waveform consisting of a bi-modal pulse applied to the acousto-optic modulator of a laser photothermal radiometric system. The horizontal time units are expressed as percentage of a full repetition period T; τ_1 and τ_2 are the corresponding square pulsewidths, and Δ is the center-to-center pulse separation. Only one repetition period is presented for clarity.

sinusoidal-wave modulation, because the LIA output signal is completely dominated by large signal baselines. A similar situation arises with the ability of laser-based frequency-domain diagnostic methodologies to monitor ion implantation doses in Si wafers. Specifically, both laser infrared photothermal radiometry (PTR) and modulated thermo- reflectance (MTR) have been shown [4] to exhibit relatively low resolution to B^+ implantation doses in the range 1×10^{12}–1×10^{13} cm^{-2}, and implantation energies 50–150 keV. In this letter we report a comparative dose-resolution study of conventional frequency-domain PTR and CMRD-PTR using 100-keV B^+, P^+, and As^+ ion-implanted industrial Si wafers, with or without surface-grown oxides in the dose range 1×10^{11}–1×10^{13} ions/cm^2. As a result of this study, details of dose-resolution advantages of CMRD-PTR are quantified.

Three sets of polished 4″ Si wafers, 10–14 Ωcm, were ion-implanted with B^+, P^+, and As^+; one set of wafers with a grown gate oxide was also implanted with As^+. Using the standard PTR experimental set-up for semiconductor metrology [5] frequency scans were performed in the range 10 Hz–100 kHz. The Ar-ion laser beam (515 nm) was focused to a spotsize of ~50 μm at an average power of 50 mW. In anticipation of very small signal variations for some wafers, stringent measures were taken to continuously monitor laser power for unwanted drifts, and PTR signal transients. The latter are known to occur upon the interaction of laser beams with unoxidized Si wafers and they constitute a form of low-activation-energy laser annealing [6]. The surface reflectivity was also monitored in a separate experiment but no measurable changes were found across the entire wafer set.

A typical set of amplitude response curves from near the center of the five unoxidized P^+-implanted wafers examined in this work is shown in Fig. 2. PTR phase curves have not been used because they are more poorly resolved with respect to implantation dose than the associated amplitudes. The low-frequency slopes in Fig. 2 are due to thermal-wave domination of the signal as a result of lattice damage by the implantation process. In the 1–100 kHz range, the photo-excited carrier plasma-wave dominates the PTR signal. The amplitude depends on the depth integral of the free-carrier-density wave and, in principle, it decreases monotonically with increasing implantation dose, as a result of enhanced recombination and trapping of photo-excited carriers at electronic defect states and traps, the density of which also increases with ion implantation dose [7]. Variations in ion-implanter parameters, however, generate non-uniform implant distributions across a wafer and diffusion-wave techniques such as PTR and MTR are sensitive to these variations [8]. In Fig. 2 it is clearly seen that signal resolution is severely compromised for doses above 4×10^{11} cm^{-2}, with the curves corresponding to 1×10^{12} cm^{-2} and 4×10^{12} cm^{-2} being essentially unresolved. Furthermore, for that particular coordinate point near the wafer center, the signal amplitude for the wafer implanted with 1×10^{13} cm^{-2} is higher than those with the two next lower doses. This trend was consistent with signals obtained from other coordinate points on these wafers. The size of experimental error bars was that of the data points in Fig. 2 and subsequent figures. Monotonic amplitude decreases with increasing dose were found, as expected, for the remaining wafers, with the exception of the B^+ wafer implanted with 4×10^{12} cm^{-2}, which showed significant amplitude increase over both the 1×10^{12} cm^{-2} and the 1×10^{13} cm^{-2} wafers. The signals from these latter wafers (center points) were very close to each other, but

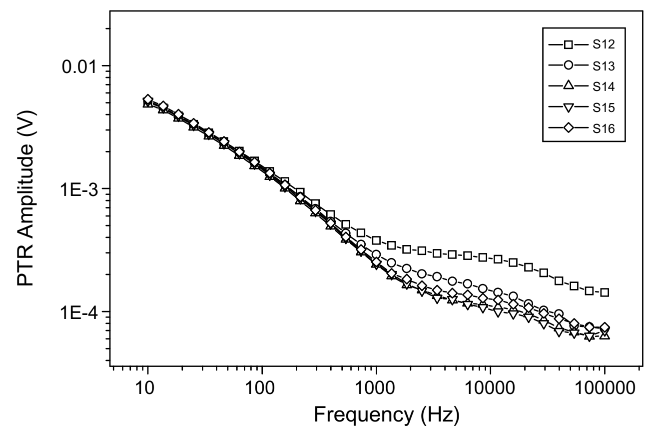

Fig. 2. PTR frequency scans of P^+ ion-implanted Si wafers at 100 keV. Doses (ions/cm^2): (□) 1×10^{11}; (○) 4×10^{11}; (△) 1×10^{12}; (▽) 4×10^{12}; (◇) 1×10^{13}.

not totally overlapped. Fig. 3 is a summary of the experimental results from the entire set of wafers at 4 kHz, a frequency at which implant dose resolution was found to be optimal for all PTR frequency scans such as those of Fig. 2. No PTR amplitude transients were observed under the laser probe, with the exception of the $1 \times 10^{11}\ cm^{-2}$ P^+- and B^+-implanted wafers. These samples exhibited very mild positive transients, slowly (~2000 s) saturating to the steady-state signal values reported in Fig. 3. With the exception of the anomalous $4 \times 10^{12}\ cm^{-2}$ B^+ and $1 \times 10^{13}\ cm^{-2}$ P^+ ion implants, the decreasing order of PTR amplitudes (B^+, P^+, As^+) for the unoxidized wafers is consistent with the increasing degree of damage incurred to the Si lattice by the progressively larger ions. It is interesting to note the relatively large restoration of PTR amplitude exhibited by the oxidized, As^+-implanted wafers, as expected from the decreased defect density at the SiO_2–Si interface [9].

The CMRD technique was applied to each wafer at the same coordinate points as the frequency scans. The repetition frequency of 4 kHz was chosen for direct comparisons with the curves of Fig. 3. Waveform center-to-center scans (separation Δ, Fig. 1) were performed with $\tau_1 = 5$ ms and $\tau_2 = 25$ ms. These pulse durations were chosen because they yielded maximum signal sensitivity. Each CMRD scan was preceded by a time-scan of the same coordinate point. It was found that the CMRD amplitude and quadrature signals were optimal in terms of dose resolution, compared to the CMRD phase and in-phase signals. Furthermore, it was established that for well-separated curves, such as those associated with the oxidized As^+-implanted wafers, there was no discernible advantage to using the CMRD over the frequency-scanned method. This is reasonable, because for large dose-generated PTR signal changes the baseline suppression ability of the CMRD is limited by the natural signal differences among PTR curves. Fig. 4 shows time scans of the 4-kHz conventional PTR signal amplitudes from the P^+-implanted wafers. Owing to the weak (or absent) transients, these traces are consistent with the order of amplitudes shown in Fig. 2 at the same frequency. The size of the increments $\delta\Delta$ controls the resolution of the technique as it limits its ability to suppress the signal baseline, i.e. to minimize the area between the [0, T/2] and the [T/2, T] pulses. $\delta\Delta = 1\%$ increments between 20% and 80% were used with only marginal improvement in resolving the overlapped P^+ $1 \times 10^{12}\ cm^{-2}$ and $4 \times 10^{12}\ cm^{-2}$ dose curves. Those scans were followed by $\delta\Delta = 0.3\%$—increment scans between 40% and 70%. The resulting curves are shown in Fig. 5. In comparison with Fig. 4, CMRD is shown to be capable of superior resolution of the $1 \times 10^{12}\ cm^{-2}$ and $4 \times 10^{12}\ cm^{-2}$ dose curves. The $4 \times 10^{11}\ cm^{-2}$ curve is also included for comparison. The curves of Fig. 5 are the smoothed averages of three experimental runs each. Smoothing was performed either by taking the average

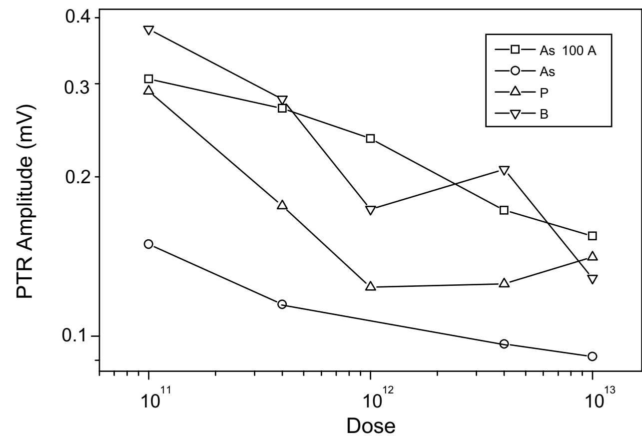

Fig. 3. PTR frequency-scan amplitude dependencies on implantation dose at 4 kHz. (□) B^+; (○) P^+; (△) As^+ (unoxidized); (▽) As^+ (with gate oxide).

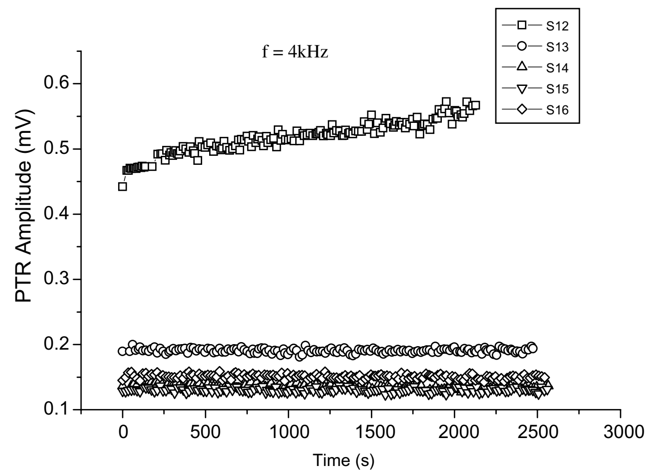

Fig. 4. Conventional square-wave modulated PTR amplitude traces from the P^+-implanted Si wafers at 4 kHz, as a function of time upon initial exposure to the laser beam. Doses (ions/cm^2): (□) 1×10^{11}; (○) 4×10^{11}; (△) 1×10^{12}; (▽) 4×10^{12}; (◇) 1×10^{13}.

over three consecutive points (discrete points) or by means of a sixth-order polynomial fit to the data (continuous lines). Smoothing may become necessary at high implant dose resolution signal levels, because the large baseline suppression of CMRD requires setting the LIA scale in the μV (instead of mV) range, where instrumental noise could be significant. The dose dependent CMRD-PTR amplitudes for P^+-implantation decrease monotonically and are shown in Fig. 6. This curve is to be compared to the corresponding conventional frequency-scanned PTR dose dependence shown in Fig. 2.

CMRD was further applied to the set of five B^+-implanted wafers. The conventional PTR time scans at 4 kHz are shown in Fig. 7. In this case the $4 \times 10^{12}\ cm^{-2}$ and $1 \times 10^{13}\ cm^{-2}$ traces are poorly resolved,

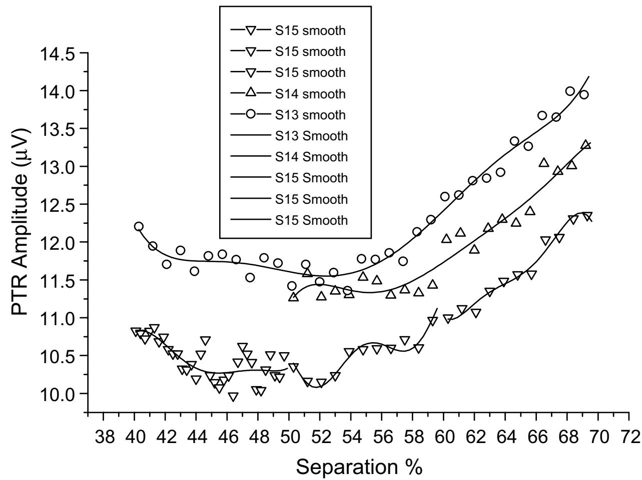

Fig. 5. PTR-CMRD amplitudes from the P^+-implanted wafers of Figs. 2 and 4 vs. pulse separation Δ (%). Doses (ions/cm^2): (▽) 4×10^{11}; (△) 1×10^{12}; (○) 4×10^{12}. Pulse separation increment $\delta\Delta = 0.3\%$.

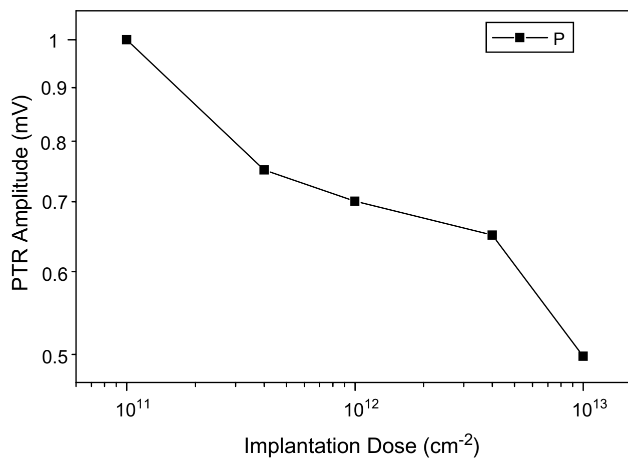

Fig. 6. High-resolution CMRD amplitudes of P^+-implanted wafers vs. implantation dose. $\delta\Delta = 0.3\%$.

however, the dose resolution is somewhat higher than that of the foregoing P^+-implants, Fig. 4. Accordingly, the CMRD technique (both amplitude and quadrature) was able to significantly improve the dose resolution of these two B^+-implanted Si wafers by use of the relatively large pulse separation increment $\delta\Delta = 1\%$. There was no need to use finer $\delta\Delta$ increments for this case, with the concomitant advantage in signal-to-noise ratio over Fig. 5. The CMRD amplitudes are shown in Fig. 8, where it is observed that the amplitude order of the various curves is the same as that of the time traces of Fig. 7 and with the B^+ curve of Fig. 3, including the "anomalously" high signal from the nominally implanted with 4×10^{12} cm^{-2} wafer.

In summary, the CMRD-PTR method has been used with B^+, P^+, and As^+, 100-keV ion-implanted Si

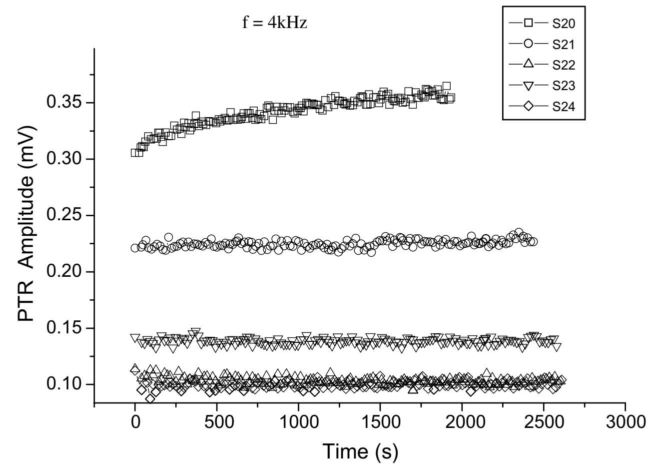

Fig. 7. Conventional square-wave modulated PTR amplitude traces from the B^+-implanted Si wafers at 4 kHz, as a function of time upon initial exposure to the laser beam. Doses (ions/cm^2): (□) 1×10^{11}; (○) 4×10^{11}; (△) 1×10^{12}; (▽) 4×10^{12}; (◇) 1×10^{13}.

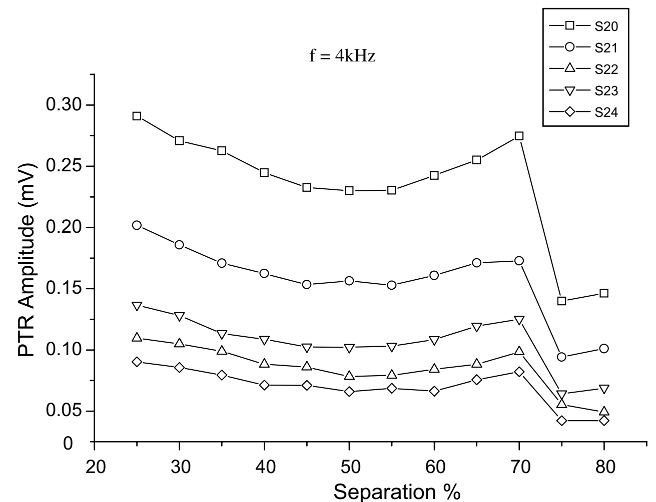

Fig. 8. PTR-CMRD amplitudes from the B^+-implanted wafers of Figs. 3 and 7 vs. pulse separation Δ (%), with $\delta\Delta = 1\%$. Doses (ions/cm^2): (□) 1×10^{11}; (○) 4×10^{11}; (△) 1×10^{12}; (▽) 4×10^{12}; (◇) 1×10^{13}.

wafers (the As^+-implants with or without surface-grown oxides) in the implantation dose range 1×10^{11}–1×10^{13} ions/cm^2. This range is difficult to monitor with conventional laser-based photothermal probes, as some signals exhibit low sensitivity to dose. It was found that CMRD can significantly enhance the dose resolution of PTR response curves from B^+ and P^+ ion-implanted wafers in cases where conventional frequency scans were totally or partially unable to resolve the dose. In all other cases where frequency scans can resolve implantation doses, CMRD did not present any significant resolution advantages. It was further established that the pulse separation increment

$\delta\Delta$ is the critical CMRD waveform parameter, which controls the dose resolution capabilities of the technique.

References

[1] Mandelis A, Paoloni S, Nicolaides L. Rev Sci Instrum 2000;71:2440.
[2] Paoloni S, Nicolaides L, Mandelis A. Rev Sci Instrum 2000;71:2445.
[3] Mandelis A. Rev Sci Instrum 1994;65:3309.
[4] Salnick A, Mandelis A, Funak F, Jean C. Appl Phys Lett 1997;71:1531.
[5] Mandelis A, Riopel Y. J Vac Sci Technol A 2000;18:705.
[6] Rodriguez ME, Garcia JA, Mandelis A, Jean C, Riopel Y. Appl Phys Lett 1999;74:2429.
[7] Rodriguez ME, Mandelis A, Pan G, Nicolaides L, Garcia JA, Riopel Y. J Electrochem Soc 2000;147:687.
[8] Rosencwaig A. In: Mandelis A, editor. Photoacoustic and thermal wave phenomena in semiconductors. New York: North-Holland; 1987 [Chapter 5].
[9] Sheard S, Somekh M. In: Mandelis A, editor. Non-destructive evaluation. Progress in photothermal and photoacoustic science and technology, vol. II. Englewood Cliffs, NJ: Prentice-Hall; 1994 [Chapter 5].